AGU PUBLICATIONS

Geochemistry, Geophysics, Geosystems

RESEARCH ARTICLE

10.1002/2014GC005310

Tectonics, topography, and river system transition in East Tibet: Insights from the sedimentary record in Taiwan

Qing Lan[1,2], Yi Yan[1], Chi-Yue Huang[1,3], Peter D. Clift[4], Xuejie Li[5], Wenhuang Chen[1], Xingchang Zhang[1], and Mengming Yu[1]

[1]Key Laboratory of Marginal Sea Geology, Guangzhou Institute of Geochemistry, Chinese Academy of Sciences, Guangzhou, China, [2]College of Earth Science, University of Chinese Academy of Sciences, Beijing, China, [3]Department of Earth Sciences, National Cheng Kung University, Taiwan, Taiwan, [4]Department of Geology and Geophysics, Louisiana State University, Baton Rouge, Louisiana, USA, [5]Key Laboratory of Marine Mineral Resources, Ministry of Land and Resources, Guangzhou Marine Geological Survey, Guangzhou, China

Key Points:

- Seafloor spreading of the South China Sea propagated from east to west after ~39 Ma
- There was a major change in the sediment provenance in Taiwan during the Late Oligocene
- Tectonic, topographic, and river system transitions in East Asia occurred at ~25 Ma

Supporting Information:

- Readme
- Auxiliary Materials 1 and 2

Correspondence to:
Y. Yan,
yanyi@gig.ac.cn

Citation:
Lan, Q., Y. Yan, C.-Y. Huang, P. D. Clift, X. Li, W. Chen, X. Zhang, and M. Yu (2014), Tectonics, topography, and river system transition in East Tibet: Insights from the sedimentary record in Taiwan, *Geochem. Geophys. Geosyst.*, *15*, 3658–3674, doi:10.1002/2014GC005310.

Received 27 FEB 2014
Accepted 17 AUG 2014
Accepted article online 26 AUG 2014
Published online 25 SEP 2014

Abstract The Cenozoic in East Asia is marked by major changes in tectonics, landscapes, and river systems, although the timing and nature of such changes remains disputed. We investigate the geochemistry and neodymium isotope character of Cenozoic mudstones spanning the breakup unconformity in the Western Foothills of Taiwan in order to constrain erosion and drainage development in southern China during the opening of the South China Sea. The La/Lu, Eu/Eu*, Th/Sc, Th/La, Cr/Th, and εNd values in these rocks show an abrupt change between ~31 and 25 Ma. Generally the higher εNd values in sediments deposited prior to 31 Ma indicate erosion from Phanerozoic granitic sources exposed in coastal South China, whereas the lower εNd values suggest that the main sources had evolved to inland southern China by ~25 Ma. The SHRIMP U-Pb ages of zircons from a tuff, together with biostratigraphy data constrain the breakup unconformity to be between ~39 and 33 Ma, suggesting that the seafloor spreading in the South China Sea commenced before ~33 Ma. This is significantly older than most of the oceanic crust preserved in the deeper part of the basin. Diachronous westward younging of the breakup unconformities and provenance changes of basins are consistent with seafloor spreading propagating from east to west. Initial spreading of the South China Sea prior to ~33 Ma corresponds to tectonic adjustment in East Asia, including extrusion of the Indochina block and the rotation and eastward retreat of the subducting Pacific Plate.

1. Introduction

Surface uplift of the Tibetan Plateau and the onset of seafloor spreading in the South China Sea are believed to have had a strong influence on the tectonics, landforms, drainage systems, and climate in East Asia during the Cenozoic [*Rowley*, 1996; *Hall*, 2002; *Wang et al.*, 2002; *Brookfield*, 1998; *Clift et al.*, 2002, 2006; *Clark et al.*, 2004]. The time at which East Asia began to tilt toward the southeast, as it does today is hotly debated. This tilting is believed to have caused the reorganization of fluvial systems in East Asia [*Li et al.*, 2001; *Clark et al.*, 2005; *Clift et al.*, 2006; *Richardson et al.*, 2008, 2010; *Yan et al.*, 2011, 2012; *Zheng et al.*, 2013]. Analyses of geomorphological pattern suggest that the modern rivers draining the Tibetan Plateau margin were once tributaries of a single, southward-flowing ancestral Red River, which drained into the South China Sea [*Brookfield*, 1998; *Clark et al.*, 2004]. In this scenario, the headwaters of the Red River were captured into neighboring basins, such as the Yangtze River as surface uplift occurred [*Clark et al.*, 2004; *Clift et al.*, 2006] (Figure 1a). However, the timing of capture is controversial. The Nd isotope composition of sediments from the Hanoi Basin together with detrital zircon age spectra from Miocene rocks in the lower Yangtze argue for the establishment of the modern drainage systems in East Tibet prior to 24 Ma [*Clift et al.*, 2006; *Zheng et al.*, 2013]. In contrast, detrital zircons and monazites in sediment cores in the modern Yangtze delta, as well as geomorphic analysis of the Yangtze at the Three Gorges have been interpreted to suggest that the Yangtze River is younger than 5 Ma [*Li et al.*, 2001; *Jia et al.*, 2010; *Yang et al.*, 2006].

Previous investigations on the topography and drainage evolution largely focused on records in terrestrial strata, which faced limitations from the discontinuous accumulation and ambiguous depositional ages [*Li et al.*, 2001; *Clark et al.*, 2004; *Zheng et al.*, 2013]. Sediments transported by rivers and deposited on the East Asia continental margins may be more reliable tracers of evolving continental erosion [*Clift et al.*, 2002,

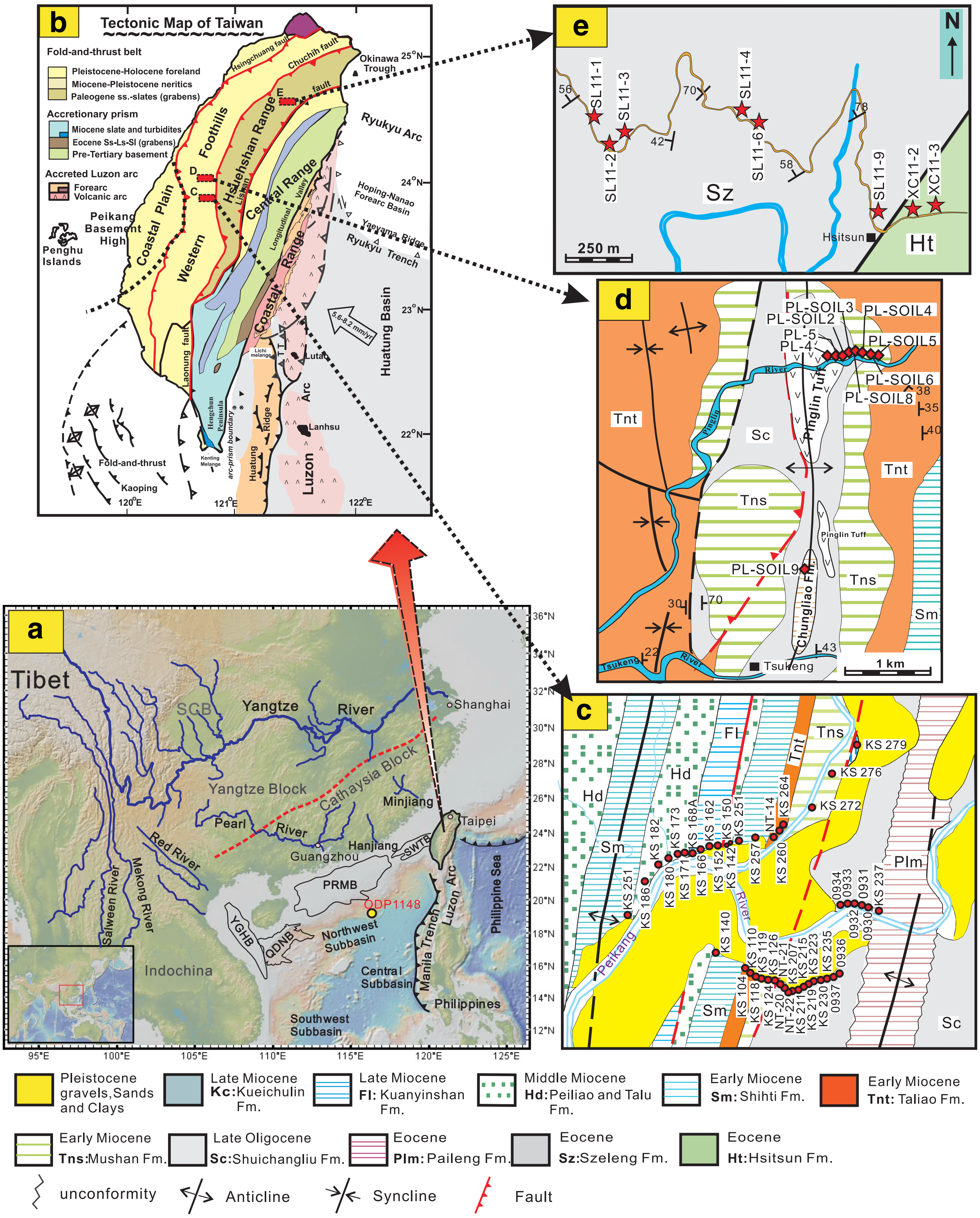

Figure 1. (a) Topographic map of eastern Tibet and the regional drainage system. YGHB: Yinggehai-Song Hong; QDNB: Qingdongnan Basins; PRMB: Pearl River Mouth Basin; SWTB: Southwest Taiwan Basin; SCB: Sichuan Basin. (b) The Tectonic Map of Taiwan is mainly based on the geological map published by Central Geological Survey, and integrates the results of *Huang* [1986] and *Huang et al*. [2012a, 2013]. The sample locations (c, d, and e) are also shown. The red circles in Figure 1c represent sample locations in Kuohsing, Western Foothills. The red diagonal squares in Figure 1d represent the sample locations in the axial section of Tsukeng Anticline of Western Foothills. The red stars in Figure 1E represent sample locations in Northern-Cross-Island Highway section, Hsuehshan range.

2006; *Li et al*., 2003; *Shao et al*., 2007] because of their continuous record and good potential for the application of biostratigraphic dating techniques [*Wang et al*., 2003]. Cenozoic sediments deposited on the northern margin of South China Sea (Figure 1a) record a change in the landscape of the Pearl and Red River basins and offer insights into the evolution of drainage in southern China and SE Tibet/SW China. Nevertheless, interpretation of provenance data from the northern margin of the South China Sea is still disputed. Nd isotope data from sediments sampled from ODP Site 1148 were interpreted by *Clift et al*. [2002] to indicate erosion from northern sources, whereas *Li et al*. [2003] favored sources to the southwest. The provenance of sediments in the northern South China Sea needs to be resolved for a better understanding of the evolution of drainage patterns and their relationship with the tectonically driven uplift in eastern Tibet.

The South China Sea lies at the confluence of the Indo-Australian, Pacific, and Eurasian plates. Its spreading history, which is still disputed, is mainly determined from magnetic anomaly lineaments [*Taylor and Hayes*, 1980, 1983; *Briais et al*., 1993; *Yao et al*., 1994; *Barckhausen and Roeser*, 2004; *Hsu et al*., 2004; *Barckhausen et al*., 2014]. *Briais et al*. [1993] argued that N-S seafloor spreading commenced at Chron 11 ($\sim$ 30 Ma) in both the northwest and central subbasins, followed by southward ridge jump at $\sim$25 Ma and the final propagation of the spreading center toward the southwest. Further studies on the magnetic anomaly lineaments in the northernmost South China Sea proposed that early seafloor spreading started at 37 Ma [*Hsu et al*., 2004]. However, *Yao et al*. [1994] and *Yao* [1997] used magnetic anomaly lineaments to conclude that both the southwest and northwest subbasins started to extend in a NE-SW direction as early as the Eocene ($\sim$ 42–35 Ma). During the transition from rifting to seafloor spreading, a breakup unconformity coinciding with the onset of seafloor spreading often develops on the rifted margins adjacent to the new oceanic crust [*Falvey*, 1974]. The onset of seafloor spreading of the South China Sea formed a series of breakup unconformities in the rifted basins including Taiwan, the Pearl River Mouth Basin, and the Qiongdongnan Basin. In this case, the age of seafloor spreading in South China Sea can theoretically be constrained by investigating the breakup unconformity in these basins [*Huang et al*., 2012b].

Taiwan is situated on the northeastern edge of the South China Sea and is largely composed of Cenozoic sequences deposited on the East Asian continental margin. These were subsequently deformed, uplifted, and exposed following arc-continent collision after 6.5 Ma [*Suppe*, 1984; *Huang et al*., 1997, 2000]. The strata exposed in Western Foothills and Hsuehshan Range correspond with units on the northern margin of South China Sea. The provenance of Cenozoic sequences in Taiwan has been addressed in a few studies which favored sources located to the northwest [*Chou*, 1980; *Tan and Youh*, 1978; *Yokoyama et al*., 2007; *Kirstein et al*., 2010; *Nagel et al*., 2013]. The sedimentary record in Taiwan offers potential clues in reconstructing the drainage evolution of southeast China. Previous studies constrained only the direction of sediment transport, but did not discuss the tectonic and geological implications.

This study addresses the provenance of sedimentary rocks exposed in the Western Foothills and Hsuehshan Range using the geochemistry of water-immobile elements such as Sc, Th, rare earth elements (REE) and their ratios, as well as Nd isotopes. These proxies have been proved to be effective to trace the sediment source [*Cullers*, 1994; *Taylor and McLennan*, 1985; *McCulloch and Wasserburg*, 1978, *Clift et al*., 2006; *Yan et al*., 2007]. Besides, our study also attempt to constrain the age of the breakup unconformity (which represents the age of initial seafloor spreading of the South China Sea) by dating zircon grains from a volcanic tuff associated with this surface. In particular, we address: (1) provenance evolution and its meaning for the tectonics of the South China Sea with regard to the timing of seafloor spreading; and (2) the relationship between regional tectonics and landform evolution since basin opening.

2. Geological Setting

The oceanic crust of South China Sea is regionally subdivided into three subbasins, the southwest, northwest, and central (or east) (Figure 1a). Large-scale rift systems developed in southeast China during Late Mesozoic-Early Cenozoic [*Yao et al*., 1994], which finally culminated in the opening of South China Sea during the Paleogene. Seafloor spreading is generally believed to have ceased during the Middle Miocene [*Briais et al*., 1993], although some studies place this slightly earlier, by $\sim$20 Ma [*Barckhausen and Roeser,* 2004*; Barckhausen et al*., 2014]. Oceanic lithosphere of the South China Sea subducted eastward beneath the Philippine Sea Plate along Manila Trench since Late Miocene, constructing the Luzon Arc [*Yang et al*., 1988, 1995]. Because the Philippine Sea Plate moved 306–332° at rates of 56–82 mm/yr [*Yu et al*., 1997] since 15 Ma, the trench must have been positioned at least 400 km east of its present location. The northern Luzon Arc eventually collided with the Asian passive margin at ~6.5 Ma [*Huang, et al*., 2000].

Taiwan is located at the juncture of the Eurasian and Philippine Sea Plates (Figure 1a) and can be divided into three tectonic domains: a fold-and-thrust belt of passive margin sedimentary rocks (including the Coast Plain, Western Foothills, and Hsuehshan Range); an accretionary prism (Hengchun Peninsula and Central Range), and a forearc basin-volcanic arc (Coastal Range) [*Huang et al*., 2012b] (Figure 1b). Within the Tsukeng Anticline (Figure 1d), *Huang et al*. [2012a, 2013] identified *Discocyclina dispansa* foraminifera and dated an interbedded tuff as Late Eocene, suggesting that the sedimentary history of the Western Foothills is much longer than previously recognized [*Ho et al*., 1956; *Ho*, 1961]. The Eocene to Late Miocene sequences can be grouped into synrift and postrift sequences (Figure 2). The former is mainly composed of thick-bedded, coarse sandstones, and siltstones of braided river and swamp facies (Figures 2 and 3a). A marine transgression is recognized and dated during the late rift stage based on the presence of foraminifera in the Paileng Formation [*Chang*, 1963; *Chiu*, 1975], as well as calcareous nannofossils in the Chungliao Formation [*Huang et al*., 2012a]. The thick Pinglin Tuff, which contains Middle Eocene calcareous nannofossils (Zone NP16), overlies a distinct unconformity between the prerifting and postrifting sequences [*Huang, et al*., 2013]. The postrift sequence is a relatively continuous Upper Oligocene to Upper Miocene shallow marine to fluvial unit. This sequence includes several transgression and regression cycles from the Late Oligocene Shuichangliu Formation to the late Middle Miocene Kuanyinshan Formation (Figures 2, and 3b–d). Shallow marine faunas are common in the postrift sequence [*Huang*, 1986] and glauconite grains are abundant in the Shuichangliu and Taliao Formations (Figure 2). The age of each formation is well constrained by foraminifera and nannofossils, as well as from the intercalated tuffs [*Huang and Cheng*, 1983; *Huang*, 1986; *Chi*, 1979; *Huang and Ting*, 1979; *Ho*, 1959; *Chang*, 1963; *Huang et al*., 2012a].

3. Sampling and Analytical Methods

In this study, we collected 60 mudstone and two volcanic tuff samples (Figures 1b–1e). Among the 60 mudstones, 45 samples were collected from the Shuichangliu stream section in Kuohsing, Western Foothills (Figure 1c), and seven from the axis of the Tsukeng Anticline (Figure 1d). Sedimentation ages are constrained by biostratigraphy. Major and trace elements, as well as Nd isotope compositions were determined for all samples. Eight mudstone samples were collected from the Eocene strata in the Hsuehshan Range (six samples from the Szeleng Formation and two samples from the Hsitsun Formation (Figure 1e)). All samples belong to the synrift unit and were analyzed for Nd isotope compositions. Two tuff samples from the Pinglin Tuff exposed within the Tsukeng Anticline were also dated.

Samples were crushed, powdered, and sieved to <75 μm fraction. They were then leached with 1 M HCl to remove biogenic/authigenic carbonate, organic matter, and Fe-Mn oxyhydroxides [*Freydier et al*., 2001] prior to analyses at the Guangzhou Institute of Geochemistry. Major element oxides were analyzed using a Rigaku RIX 2000 X-ray fluorescence spectrometer on fused glass beads. Calibration lines used in quantification were produced by bivariate regression of data from 36 reference materials encompassing a wide range of silicate compositions [*Li et al*., 2005], and analytical uncertainties are between 1% and 5%. Trace elements, including REEs, were determined by a PerkinElmer Sciex ELAN 6000 inductively coupled plasma mass spectrometer (ICP-MS). Analytical procedures are similar to those described by *Li et al*. [2000]. About 40 mg of powdered sample was dissolved in a high-pressure Teflon bomb for 24 h using a HF + HNO_3 mixture. An internal standard solution containing the single element Rh was used to monitor signal drift during counting. A set of USGS and Chinese national rock standards including BHVO-1, W-2, AGV-1, G-2, GSR-1, and GSR-3 were chosen to calibrate concentrations. The analytical precision is 5–10%. Nd isotopic compositions were determined using a Micromass Isoprobe multicollector ICP-MS, using the methods of *Li et al.* [2004]. Nd was separated by column chemistry and then analyzed. Measured $^{143}Nd/^{144}Nd$ ratios were normalized to $^{146}Nd/^{144}Nd = 0.7219$ and the reported $^{143}Nd/^{144}Nd$ ratios were further adjusted relative to the Shin Etsu JNdi-1 standard of 0.512115.

The zircons obtained from the two tuff samples were handpicked and mounted in transparent epoxy resin and polished to expose the core of the grains. Cathodoluminescence (CL) images were obtained using a CAMECA electron microprobe at the Institute of Geology and Geophysics, Chinese Academy of Sciences

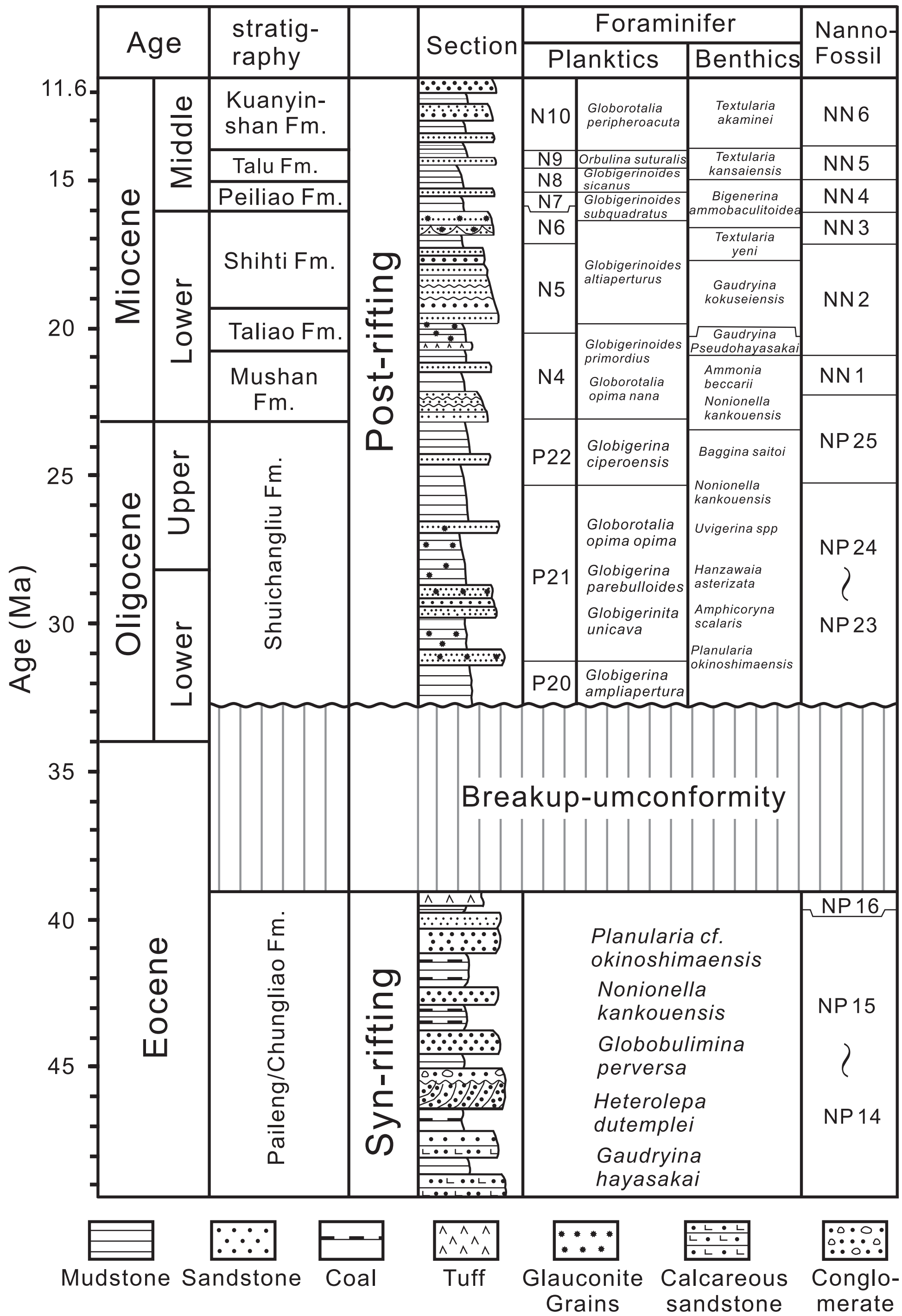

Figure 2. Stratigraphic column in the Western Foothills. The data on Foraminifers and Calcareous Nannofossils are cited from *Huang and Cheng* [1983], *Huang* [1986], *Huang and Ting* [1979], and *Chi* [1979].

(IGGCAS) in Beijing, in order to identify internal structures and choose potential target sites for U-Pb analyses. U-Pb dating of zircons was performed using a CAMECA IMS-1280 ion microprobe (CASIMS) at IGGCAS, following the analytical procedures described in *Li et al.* [2009]. U-Th-Pb abundances and their isotopic ratios were determined relative to the standard zircon 91500 [*Wiedenbeck et al.*, 1995]. The analyses were interspersed with those of unknown grains. The age data are represented in Tera-Wasserburg diagrams [*Tera and Wasserburg*, 1972].

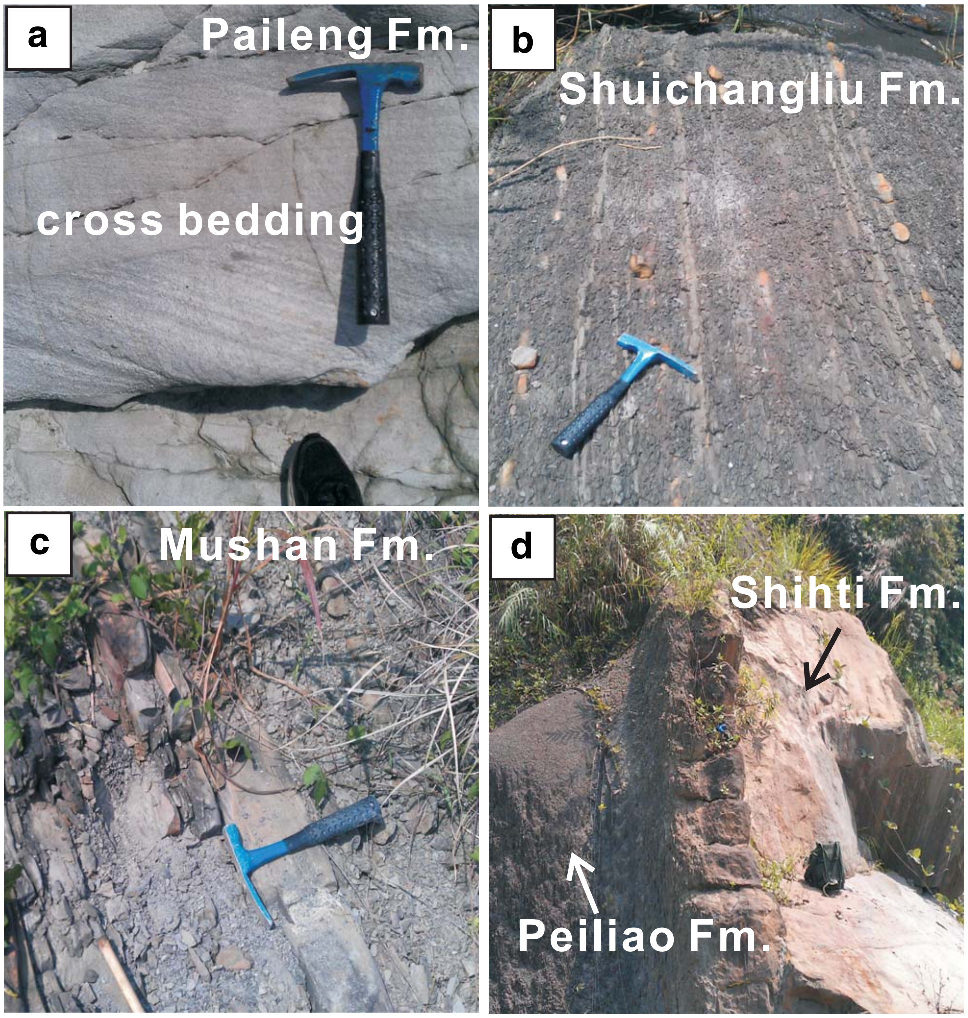

Figure 3. Photographs of the outcrops showing the stratigraphy in Western Foothills of Taiwan. (a) Sandstone with cross bedding in Eocene Paileng Formations; (b) siltstones and shales interbedded in Oligocene Shuichangliu Formation; (c) sandstones intercalated with shale and siltstone beds in Lower Miocene Mushan Formation; (d) thick sandstone in Lower Miocene Shihti Formation and the calcareous mudstone of Middle Miocene Peiliao Formation.

4. Results

Results of major and trace element contents, as well as Nd isotope analyses are listed in supporting information S1. The Post-Archean Australian Shale (PAAS) [*Taylor and McLennan*, 1985], which represents the average composition of upper crust, is used to determine the enrichment or loss of major and trace elements in mudstones. The zircon U-Pb age data are shown in supporting information S2.

4.1. Major Elements

The major element composition reflects the mineralogy of each sample. Mudstones from the Western Foothills have SiO_2 concentrations ranging from 60.58 to 78.91 wt %. Most samples have higher SiO_2 contents than those of the PAAS. The Eocene to Upper Oligocene mudstones have higher SiO_2 (average 72.5 wt %) than that of the Miocene samples (average 66.0 wt %) (Figure 4). The concentrations of MnO and Fe_2O_3 are below those of PAAS. The concentration of Al_2O_3 ranges from 11.96 to 21.20 wt %, which is lower than that of PAAS, except for three samples from the Shihti (KS140), Taliao (KS118), and Mushan (PL-SOIL5) Formations. In addition, the Eocene and Upper Oligocene samples have lower TiO_2 and higher K_2O/Na_2O than those of the Miocene samples (Figure 4).

4.2. Trace Elements

Compared with PAAS, all samples from the Western Foothills have lower Sc, V, Ni, Co contents but similar Cr mean contents. The Rb, Cs, Th, and U contents show limited ranges and average contents similar to those

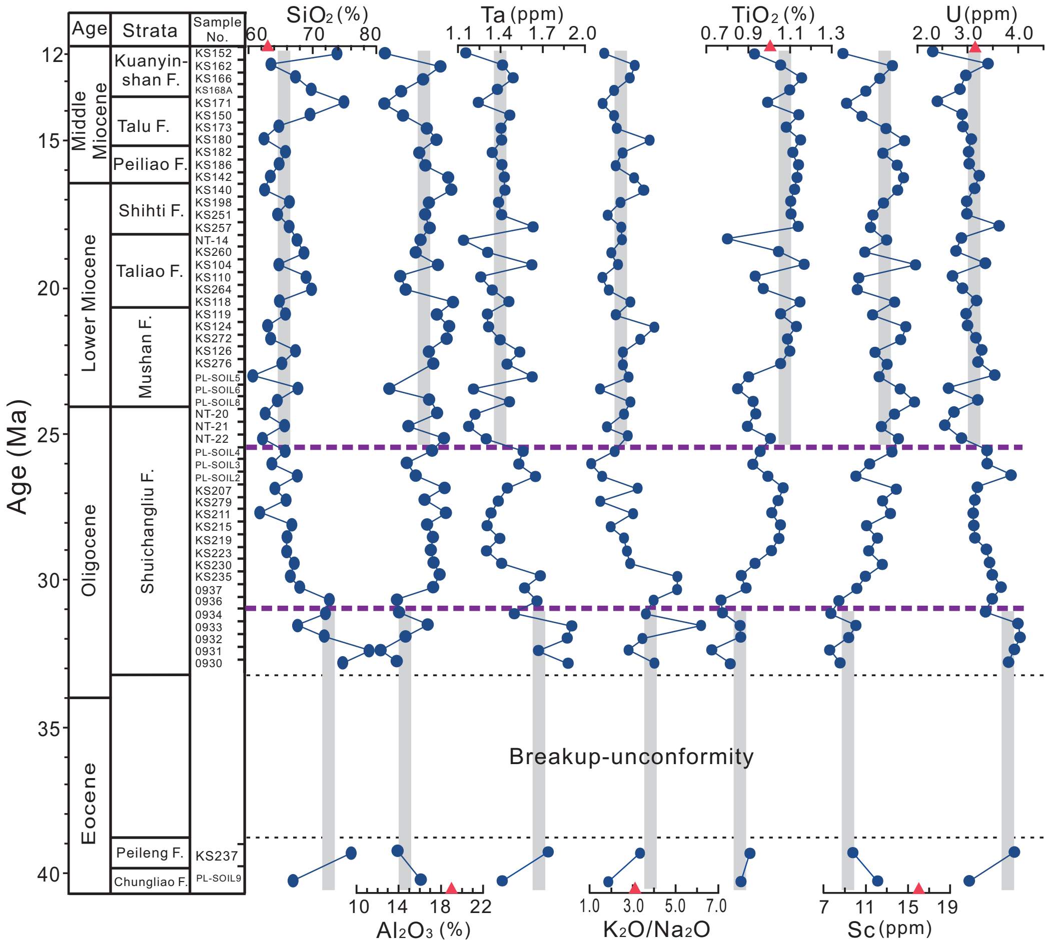

Figure 4. The compositional variation of SiO_2, Al_2O_3, K_2O/Na_2O, TiO_2, Ta, Sc, and U for mudstones in Western Foothills. The red triangles represent the values of PAAS [*Taylor and McLennan*, 1985]. The gray lines represent the average variation trend of major and trace elements prior to ~ 31 Ma and after ~ 25 Ma.

of PAAS. Unlike Cr, Sr, U, and Th, the V, Ni, Co, and Rb concentrations show clear positive correlations with Al_2O_3 ($r \geq 0.5$). Cs and Ba have moderate correlation coefficients ($r = 0.44$ and 0.35, respectively; Table 1).

Y and Nb have lower average concentrations than those of PAAS (0.85 × PAAS, 0.91 × PAAS, respectively). La, Y, Nb, and Th show poor correlation with SiO_2 concentrations (Table 1). Th does not show any marked correlation with Zr and CaO. Cr has very weak correlation with most other elements, such as Zr, Y, CaO, and Al_2O_3 (Table 1). The Sc, Ti, Ta, and U in Upper Oligocene samples (31–25 Ma) show a major change with average concentrations of 9.20, 4165, 1.68, and 3.68 ppm, respectively, in the samples with ages older than ~31 Ma. However, these values show different concentrations (12.71, 7266, 1.37, and 2.99 ppm, respectively) in post ~25 Ma samples (Figure 4).

4.3. Rare Earth Elements

The $\sum$REE concentrations of the mudstones are broadly similar to that of PAAS, with the exception of two samples from the Paileng (KS237) and Mushan (PL-SOIL5) Formations in having much higher $\sum$REE. All samples show $(La/Yb)_N$ values higher than those of PAAS, indicating that the mudstones are relatively enriched in LREEs. Furthermore, the Eu/Eu* ranges from 0.47 to 0.66, with an average value of 0.59, which is slightly lower than that of PAAS (0.65). The Yb and $\sum$REE display a weak correlation with Zr ($r = 0.34$, -0.1), whereas La and Hf show poor correlation coefficient ($r = 0.18$) (Table 1). The average chondrite-normalized REE concentration plots for each sedimentary unit (Figure 5) demonstrate typical upper crustal composition, with LREE enrichment, HREE depletion, and a negative Eu anomaly.

Table 1. Correlation Coefficients (r) From the Correlation Matrix Obtained With Geochemical Data of Mudstones in Western Foothills[a]

r	Al_2O_3	CaO	P_2O_5	TiO_2	Y	Zr	Nb	La	Th
SiO_2	−0.86	−0.28	−0.06	−0.53	−0.09	**0.84**	−0.05	−0.39	−0.15
Rb	**0.68**	−0.03	0.08	0.35	0.19	−0.54	**0.59**	0.46	0.43
Th	0.3	0	0.32	−0.31	**0.64**	0	**0.58**	**0.59**	**1**
U	0.11	−0.27	0.17	−0.29	0.47	0.28	**0.76**	0.37	**0.75**
Sc	**0.7**	0.13	−0.04	**0.56**	0.14	−0.7	0	0.38	0.04
V	**0.69**	0.18	0	**0.79**	0	−0.72	0.08	0.34	−0.13
Sr	−0.05	**0.76**	0.39	0	0.02	−0.31	−0.16	0.16	0.14
Cr	0.02	0.01	0.01	0.01	−0.02	−0.06	−0.24	0.04	−0.1
Co	0.48	0.31	0.16	0.38	−0.17	−0.67	−0.32	0.04	−0.12
Ni	**0.56**	0.31	0.13	0.46	−0.15	−0.7	−0.24	0.1	−0.11
Ba	0.35	0	−0.31	0.39	−0.16	−0.42	−0.18	0.12	−0.36
Cs	0.44	−0.09	0.15	0.27	0.36	−0.31	**0.61**	0.48	0.48
Hf	−0.65	−0.26	−0.15	−0.51	0.17	**0.99**	0.14	−0.18	0.09
Yb	0.17	−0.35	0.02	−0.12	**0.92**	0.34	**0.58**	**0.71**	**0.64**
Eu/Eu*	0.26	0.25	0.06	**0.57**	−0.28	−0.68	−0.35	−0.03	−0.48
La/Lu	**0.56**	0.33	0.13	0.45	−0.03	−0.65	−0.22	0.47	0
Th/La	−0.23	0.06	0.23	−0.56	−0.05	0.27	0.33	−0.3	**0.58**
Th/Cr	0.08	−0.06	0.11	−0.28	0.3	0.13	**0.51**	0.18	**0.6**
Th/Sc	−0.38	−0.14	0.23	−0.66	0.29	**0.57**	0.39	0.05	**0.62**
∑REE	0.46	−0.12	0.15	0.03	**0.9**	−0.1	0.37	**0.98**	**0.68**
LREE	0.48	−0.11	0.15	0.04	**0.88**	−0.13	0.37	**0.98**	**0.67**
HREE	0.22	−0.19	0.14	−0.1	**0.98**	0.17	0.39	**0.82**	**0.68**
$(La/Yb)_N$[b]	**0.54**	0.31	0.12	0.37	−0.07	−0.7	−0.24	0.44	−0.01

[a]The correlation coefficients greater than 0.5 are shown in bold.
[b]$(La/Yb)_N$ means the chondrite-normalized La/Yb ratio.

4.4. Element Ratios

Variations in trace element ratios in mudstones are shown in Figure 6. Although the two Eocene samples from the Paileng (KS237) and Chungliao (PL-SOIL9) Formations show little variation in elemental ratios, they are similar to the oldest samples from the Oligocene. The La/Lu, Eu/Eu*, Th/Sc, Th/La, and Cr/Th show major changes within the Oligocene (~ 31–25 Ma). The La/Lu of mudstone increases abruptly from 72.33–105.17 to 94.79–123.4 during the time of 31 Ma to <25 Ma. At the same time, the Eu/Eu* shows an increase from 0.47–0.58 to 0.50–0.65. In contrast, the ratios of Th/Sc, Th/La, and Cr/Th show higher values for samples older than ~31 Ma as compared with those younger than ~25 Ma (Figure 6).

The values of Th/Sc, Th/La, and Cr/Th of mudstone samples from the Oligocene Shuichangliu Formation show coherent decrease, in contrast with the increase in Eu/Eu* and La/Lu upsection. A couple of samples from the Mushan Formation show markedly different values of La/Lu, Eu/Eu*, and Th/Sc as compared to those immediately above and below. However, such variation is absent in Th/La and Cr/Th values. The Middle Miocene samples display little variation in La/Lu, Th/Sc, and Th/La (Figure 6).

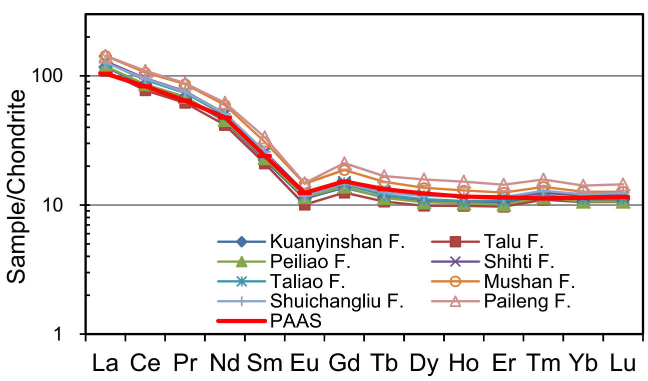

Figure 5. The average chondrite-normalized REE distribution plot for each stratigraphic unit (the chondrite values are cited from *Taylor and McLennan* [1985]).

4.5. Nd Isotopes

The $^{143}Nd/^{144}Nd$ ratios of mudstones range from 0.511877 to 0.512157 (Figure 7). Although there is a general uneven trend to more negative values, most of the Eocene samples possess higher εNd values than those of the younger sediments, ranging between −11.80 and −10.0. Despite the time gap of the breakup unconformity, the lowest Oligocene (>31 Ma) samples have even higher εNd isotope value than that of the underlying Eocene samples. However, they show a coherent decrease upsection until ~27 Ma

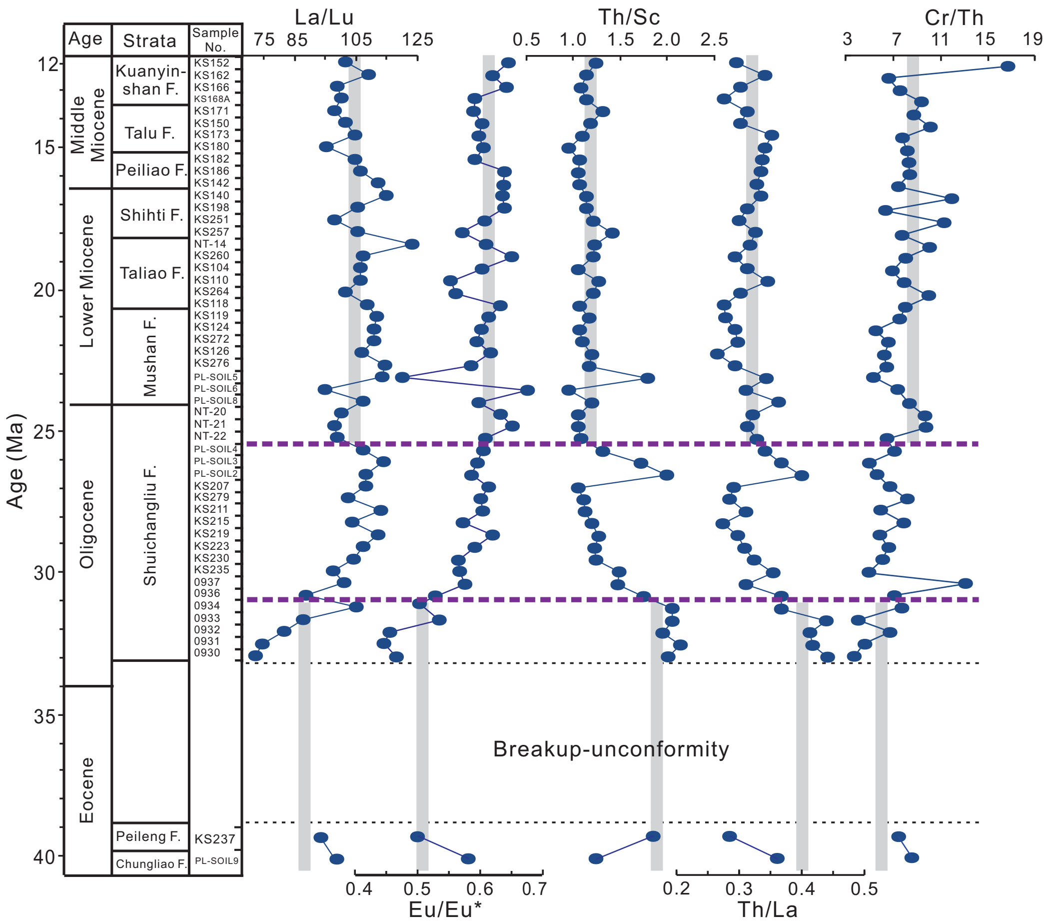

Figure 6. The variation of element ratios with age for mudstones in Western Foothills. The Cr/Th, La/Lu, Th/Sc, Eu/Eu*, and Th/La show a sharp shift during Upper Oligocene. The gray lines represent the average variation trend of element ratios prior to ~ 31Ma and after ~ 25Ma.

(εNd of −14.84 in the Shuichangliu Formation). Between 27 and 25 Ma, the εNd values are erratic with an initial sharp increase before falling and stabilizing after 25 Ma, ranging from −14.5 to 11.9 (with an average value of −13.0). The εNd values show a gentle shift to more negative values during the Early Miocene but after ~15 Ma, these show limited variability, without regaining the high values seen in the synrift sequence (Figure 7).

4.6. SHRIMP U-Pb Ages of Zircons From the Volcanic Tuff

The Tera-Wasserburg diagrams and part CL images of zircons from the Pinglin Tuff are shown in Figure 9. Most of the zircons show oscillatory zoning under CL, typical of an igneous origin [*Fedo et al.*, 2003; *Wu et al.*, 2010]. The samples PL-4 and PL-5 are dated as 39.79 ± 0.39 Ma and 39.53 ± 0.44 Ma, respectively (Figure 9), which indicate the breakup unconformity had already formed at least at ~ 39 Ma. Together with the detailed biostratigraphy above and below the breakup unconformity [*Huang et al.*, 2012a], the age of the breakup unconformity could be constrained to be between ~33 and ~39 Ma.

5. Discussion

5.1. Provenance

5.1.1. Influence of Marine Authigenic Minerals and Hydraulic Sorting

Since the Nd isotopic composition of sedimentary rocks is influenced by Fe-Mn oxyhydroxides [*Wei et al.*, 2004], the Nd isotopic composition of samples with abundant authigenic materials are unrepresentative of their provenance [*Li et al.*, 2003; *Yan et al.*, 2007]. The mudstone samples were leached with 1 M HCl to

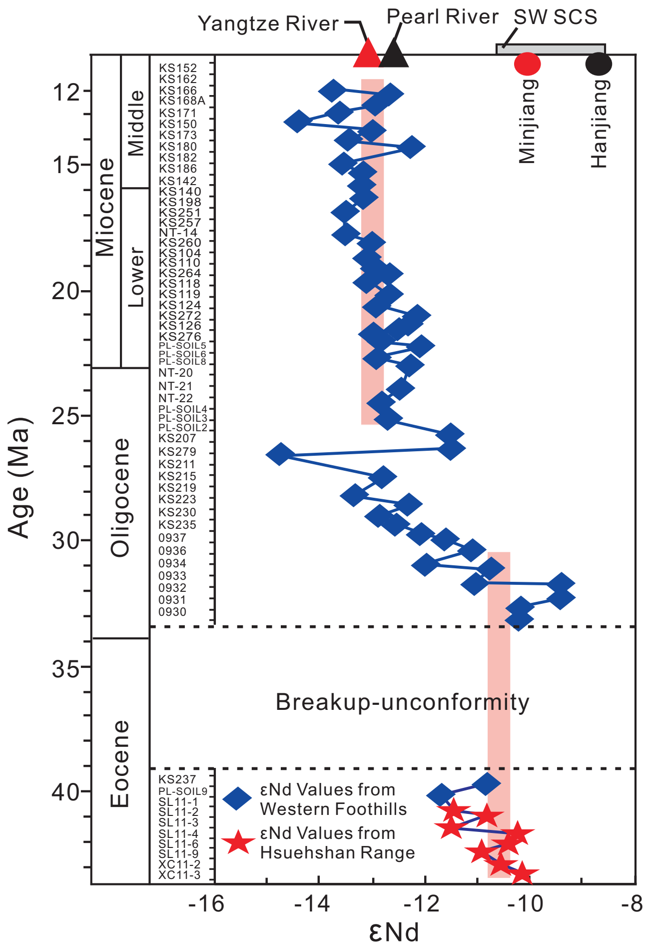

Figure 7. The profile variations of Nd isotopic composition of mudstone in Taiwan, compared with modern river εNd values from Yangtze River [*Yang et al.*, 2007], Minjiang and Hanjiang [*Shao et al.*, 2009], Pearl River [*Shao et al.*, 2007; *Hu et al.*, 2013], and Southwest South China Sea [*Li et al.*, 2003 and references therein]. The pink lines represent the average variation trend of εNd isotope ratios prior to ~ 31Ma and after ~ 25Ma. The present value for CHUR reservoir is 143Nd/144Nd = 0.512638 from *Hamilton et al.* [1983]. SW SCS: Southwest South China Sea.

remove the biogenic/authigenic content (carbonate, organic matter, and Fe-Mn oxyhydroxides) [*Freydier et al.*, 2001]. Although minor Fe-Mn oxyhydroxide, organic matter, and authigenic opal may remain in the residue, their abundance is very low, as shown by the low contents of CaO and MnO (average 0.27 and 0.02 wt %, respectively), lower than those of PAAS.

The stable accessory mineral, such as quartz (SiO_2), zircon ($ZrSiO_4$), and apatite (phosphate), would enrich in sedimentary rocks during hydraulic sorting. These enriching accessory minerals may result in the geochemical change of sedimentary rocks. For example, zircon accumulation usually causes slight enrichment in Zr, Th, and heavy rare earth elements [*Cullers*, 1994]. The $\sum$REE concentrations of the mudstones in this study are broadly similar to that of PAAS. La and Th have poor correlation with SiO_2 concentrations, indicating that hydraulic sorting has little influence on these elements. In addition, LREE and $\sum$REE show weak correlation with P_2O_5 and Zr indicating that these have not been influenced by the modal content of apatite or zircon. During sediment transport, some weathering-resistant minerals may get concentrated by sorting, causing enrichment of REEs [*Cullers et al.*, 1979]. Two samples from the Paileng (KS237) and Mushan (PL-SOIL5) Formations are exceptional in having much higher $\sum$REE compositions than those of PAAS (Figure 5), suggesting that these two samples are likely influenced by enrichment in heavy minerals. A small number of samples from the Mushan and Shuichangliu Formations show prominent changes in some elemental ratios, but the temporal trend in these is not consistent or long lasting. For instance, sample PL-SOIL2 from the Upper Shuichangliu Formation shows higher Th/Sc and Th/La than those in the samples above and below, but the La/Lu, Eu/Eu*, and Cr/Th values do not show this trend (Figure 6). Such changes in elemental ratios are not mirrored in Nd isotope compositions. In summary, the geochemical composition of the mudstones is not significantly influenced by hydraulic sorting except the two samples from the Paileng (KS237) and Mushan (PL-SOIL5) Formations, so that our geochemical proxies can be considered robust for constraining the provenance.

5.1.2. Geochemical Response to Provenance Change

Although small variations are seen, the element ratios of mudstones show marked change in a coherent fashion between ~ 31 and 25 Ma. A comparison of La/Sc, Th/Sc, Cr/Th, and Co/Th ratios of mudstones in Taiwan with those in sediments derived from granites, andesites, mafic, and felsic sources (Table 2), suggests a prominent change of provenance. Samples older than 31 Ma have higher La/Sc and Th/Sc ratios and lower Cr/Th, Eu/Eu*, and Co/Th ratios as compared with those younger than 25 Ma (Table 2). Because of the enrichment in Th and La within silicic rocks and Sc, Cr, and Co in basic rocks [*Cullers*, 1994], the low

Table 2. Ranges of Elemental Ratios in the Mudstones From Taiwan Compared With the Analogous Ratios in Sediments Derived From Granites, Andesites, and Sediments From Mafic and Felsic Sources

					Late Oligocene – Miocene (Post-25 Ma)		Eocene-Late Oligocene (Pre-31 Ma)	
Elemental Ratio	Granites[a]	Andesites[a]	Sediments From Mafic Sources[b]	Sediments From Felsic Sources[b]	Range	Average	Range	Average
La/Sc	8	0.9	0.43–0.86	2.5–16.3	2.77–5.21	3.7	3.43–6.48	4.93
Th/Sc	3.57	0.22	0.05–0.22	0.84–20.5	0.95–1.79	1.16	1.24–2.13	1.89
Cr/Th	0.44	9.77	25–500	4.00–15.0	5.39–16.87	8.43	3.69–8.66	6.17
Co/Th	0.17	4.65	7.1–8.3	0.22–1.5	0.34–0.85	0.55	0.05–0.48	0.19
Eu/Eu*	0.34	0.66	0.71–0.95	0.4–0.94	0.5–0.67	0.61	0.47–0.58	0.51

[a] *Condie* [1993].
[b] *Cullers* [1994, 2000] and *Cullers and Podkovyrov* [2000].

Cr/Th ratios can be interpreted to indicate more sediment flux from acid igneous sources (such as granites) in pre-31 Ma mudstones. We infer erosion from the large areas of Phanerozoic granite exposed in southeastern China before ~31 Ma. Subsequently, the degree of erosional flux from acid igneous rocks decreased (higher Co/Th, Cr/Th, Eu/Eu*, and lower Th/Sc and La/Sc), indicating a changing provenance.

5.1.3. Nd Isotopic Response to Provenance Change

Except for the abrupt rise in Nd isotopes upsection displayed by the Oligocene sample (PL-SOIL2), the general temporal trend in εNd is from −10.5 prior to ~31 Ma to −13.0 after ~25 Ma, marking a transition during 31 to 25 Ma (Figure 7). The basement rocks in the Cathaysia Block have generally higher εNd values than those of the adjacent Yangtze Block. This is mainly due to the extensive Mesozoic arc magmatism in the Cathaysia Block [*Gilder* et al., 1996; *Darbyshire and Sewell*, 1997], as compared to the dominantly Precambrian crust in the latter [*Ma et al*., 2000] (Figure 8). Nonetheless, the blocks are not homogenous and the Phanerozoic arcs of SE Cathaysia have more positive εNd values than the interior of this block [*Chen and Jahn*, 1998]. The εNd values show a prominent shift to more negative values during the Early Miocene, which might indicate the gradually increasing flux from inland China. Because the isotopically more positive arc rocks are concentrated along the SE coast of Cathaysia, the change of source area in Cenozoic sedimentary rocks in Taiwan from coast to interior could reflect more drainage from the interior of this block. The εNd values show limited variability after ~15 Ma, which is similar to that seen at ODP Site 1148 [*Li et al*., 2003; *Clift et al*., 2002]. We interpret these isotopic jumps to possibly reflect the Dongsha Movement on the northern margin [*Lüdmann and Wong*, 1999], but the isotopic evolution may simply reflect the growth and amalgamation of rift-related drainage system inland following the continental breakup.

For comparison, we compiled the Nd isotopic ratios of sediments and bedrocks surrounding Taiwan, including those from the Cathaysia Block, Yangtze Block, South China Continental Shelf (Minjiang and Hanjiang), the modern Pearl River, and Southwest South China Sea [*Hu et al*., 2013; *Chen and Jahn*, 1998; *Li et al*., 2003] (Figures 7 and 8). It is possible that the southwestern areas of South China Sea, such as offshore Borneo, Sunda Shelf, and offshore Indochina could have served as source areas for the sediments in Taiwan before ~31 Ma, as proposed by *Li et al*. [2003]. However, the geochemistry of sediments in Indochina is characterized by lower La/Sc (4.2) and Cr/Th (1.09), and higher Th/Sc (1.46) and Co/Th (0.55) [*Lan et al*., 2003] compared to our pre-31 Ma mudstones (5.18, 6.17, 0.18, and 0.19, respectively). This lack of geochemical correlation and the paleogeography that identifies a rift between the sources and the Taiwan basin argue against sediment flux from the southwest. Meanwhile, evidence from the Yinggehai-Song Hong, Qiongdongnan, and Pearl River Mouth Basins clearly identify northern sediment sources during that time [*Yan et al*., 2007; *Shao et al*., 2007]. In addition, monazite ages in Eocene to Oligocene sandstones from Taiwan [*Yokoyama et al*., 2007] do not support a southwest provenance

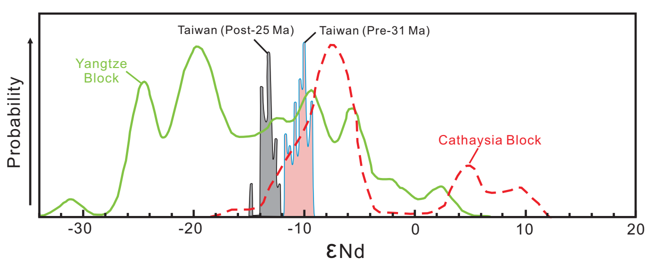

Figure 8. Relative probability plots of Nd isotopic compositional ranges of Yangtze and Cathaysia Blocks [*Clift et al*., 2006 and references therein] and pre-31 Ma and post-25 Ma samples derived from Taiwan.

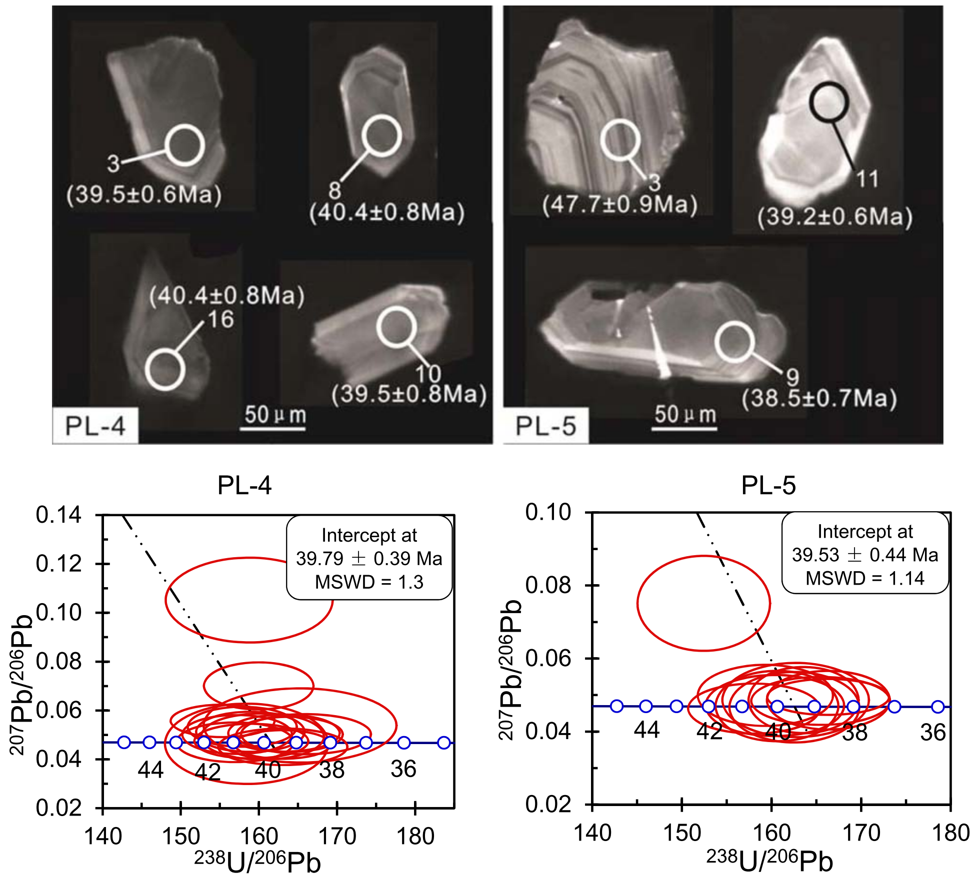

Figure 9. Cathodoluminescence (CL) images of zircons in Pinglin Tuff and Tera-Wasserburg plots of SHRIMP U-Pb ages.

because they lack Precambrian and Triassic grains, which are abundant on the Indochina-Sunda Shelf and northwestern Borneo. Therefore, our data support the model of *Clift et al*. [2002] that favors a dominant Cathaysian provenance before ~31 Ma to the southern Chinese margin.

The locus of erosion would have migrated inland especially between ~31 and 25 Ma. Although the primitive arc rocks of coastal Cathaysia still provided material to that part of the southern Chinese margin which subsequently became Taiwan, the percentage of materials derived from either the Yangtze Block or the interior of Cathaysia increased significantly after ~25 Ma. The lower εNd values of mudstones generally postdate ~25 Ma and require sediments with more negative Nd isotope values to balance the more positive εNd from coastal Cathaysia sources. The Yangtze Block or the interior of Cathaysia could have provided this material (Figure 8).

A comparison of the Nd isotopic values of mudstones from Taiwan with sediments derived from the estuaries of major rivers in eastern China, including the Hanjiang, Minjiang, Pearl, and Yangtze Rivers (Figure 7), demonstrates that the εNd values of the Minjiang (εNd = −9.6) and Hanjiang (εNd = −8.6) [*Shao et al*., 2009] are similar to those of pre-31 Ma sediments in Taiwan. This feature suggests that the coastal Cathaysia Block, which these two rivers now drain, could have been the main source to the Taiwan part of the margin before 31 Ma. However, the Nd isotopic compositions show values closer to those of the sediments from the Yangtze (εNd = −13) [*Yang et al*., 2007] and Pearl River Mouth (εNd = −10 to −12) [*Shao et al*., 2007; *Hu et al*., 2013] after ~25 Ma. The two rivers traverse the Yangtze Block and the interior of the Cathaysia Block, respectively, with the Pearl only draining a small part of the Yangtze Block in the far west of its basin. This implies that either of these provenances could have been the active contributor after 25 Ma. Therefore, we conclude that the westward expansion of the Yangtze or Pearl Rivers had already reached the interior of Cathaysia or the Yangtze Block starting from ~ 31 Ma, and that the westward expansion of drainage stabilized after ~ 25 Ma. The isotopic change after ~ 31 Ma could indicate that the coastal mountains in SE

China [*Wang*, 1998, 2005; *Chen*, 2000] had reduced and that east-tilting topography had begun to develop, although it should be noted that the area of drainage capture in SW China lies outside the Pearl River basin and would not have directly affected sediment flow to the Taiwan region. Nonetheless, the change of provenance from the southern Chinese coast before 31 Ma to erosion of sources from more inland areas after 25 Ma corresponds to the transition of landscapes and fluvial systems seen elsewhere in East Asia [*Clift et al*., 2006; *Zheng et al*., 2013].

5.2. Age of Oceanic Crust and the Opening of the South China Sea

We link the unconformity in the Tsukeng Anticline of the Western Foothills, marked by the Pinglin Tuff, to the breakup event [*Huang et al*., 2012a]. Below the unconformity, thick-bedded coarse sandstones and siltstones of braided river and swamp facies correspond to the period of rifting. The presence of foraminifers and calcareous nannofossils in the upper parts of the synrift sequence testifies to occasional marine transgressions. Above the Pinglin Tuff, shallow marine and fluvial strata were deposited without significant stratigraphic break reflecting thermal subsidence dominating the vertical tectonics.

SHRIMP U-Pb dating of zircons from the Pinglin Tuff (Figure 9) and detailed biostratigraphy above and below the breakup unconformity [*Huang et al*., 2012a] constrain the breakup unconformity to between ~33 and ~ 39 Ma, which represent the time of initial opening of the South China Sea. Thus, the age of initial spreading is older than the age of known oceanic crust of South China Sea, and is similar to the age proposed by *Hsu et al*. [2004] in the northeast basin, adjacent to our section.

Previous studies have demonstrated diachronous breakup unconformities in the northern South China Sea. For example, the ages of the breakup unconformities in the Pearl River Mouth Basin is ~30 Ma, the Qiongdongnan Basin is ~ 23 Ma [*Zhou et al*., 1995], while in Taiwan it is >33 Ma (Figure 10a). A similar trend for the breakup unconformity with younging from east to west is seen on the south margin of the South China Sea [*Liu et al*., 2012].

The evolution of sediment into these basins reflects the opening of the South China Sea and the subsequent drainage evolution after the culmination of extension. The changes in εNd values in basins in the northern South China Sea (Figure 10b) show that the provenance, like the age of breakup unconformities, is diachronous. The transition of provenance shows younging from the eastern to the western basins. If the provenance change is understood to be a delayed response of drainage to rifting, the progression of ages can be interpreted to reflect rift propagation. In Taiwan, the provenance changes at ~31–25 Ma, while at ODP Site 1148 and in the Pearl River Mouth Basin, the change is at ~27–23 Ma [*Clift et al*., 2002; *Li et al*., 2003; *Shao et al*., 2007]. Furthermore, this transition occurred in the Yinggehai-Song Hong and Qiongdongnan Basins at ~13 Ma [*Yan et al*., 2007] (Figure 10b). The diachronism of the breakup unconformities, together with the transition of provenances, could reflect the propagation of seafloor spreading that commenced earlier in the east (>33 Ma) than in the west (~23 Ma). Strike-slip motion along the Red River Fault Zone has been widely regarded as accommodating the convergence between India and Eurasia [*Tapponnier et al*., 1986; *Peltzer and Tapponnier*, 1988]. Thermochronological studies indicate that faulting and exhumation started at around 34 Ma [*Leloup et al*., 2001; *Gilley et al*., 2003]. The eastward extrusion of Indochina along the Ailao Shan-Red River Shear Zone not only accommodates a substantial part of the convergence between India and Eurasia, but may in part be responsible for the opening of the South China Sea, although some workers argue that there is little indication that India has been the driving force of tectonics in most of SE Asia [e.g., *Hall*, 2002]. The Pacific Plate has undergone a major kinematic reorganization at around 43 Ma, involving a 50° rotation from a NNW to WNW trajectory manifested in the change of orientation of the Hawaiian-Emperor Islands volcanic chain [*Sharp and Clague*, 2006].

5.3. The Evolution of Landscapes and Fluvial Systems in East Asia

The uplift of the Tibetan Plateau coupled with the opening of the marginal seas must have had important impact in changing landscapes and drainage systems, which would have triggered changes of provenance in the continental margins in East Asia, albeit not as far east as Taiwan. Previous studies based largely on geomorphological patterns have shown that the modern rivers draining the plateau margin may have once been the tributaries to a single, southward flowing river into the ancestral Red River, which drained into the South China Sea [*Brookfield*, 1998; *Clark et al*., 2004] Nd isotopic composition and Pb isotope data of sediments derived from the Hanoi Basin by *Clift et al*. [2006] and *Hoang et al*. [2009] suggested that the Yangtze

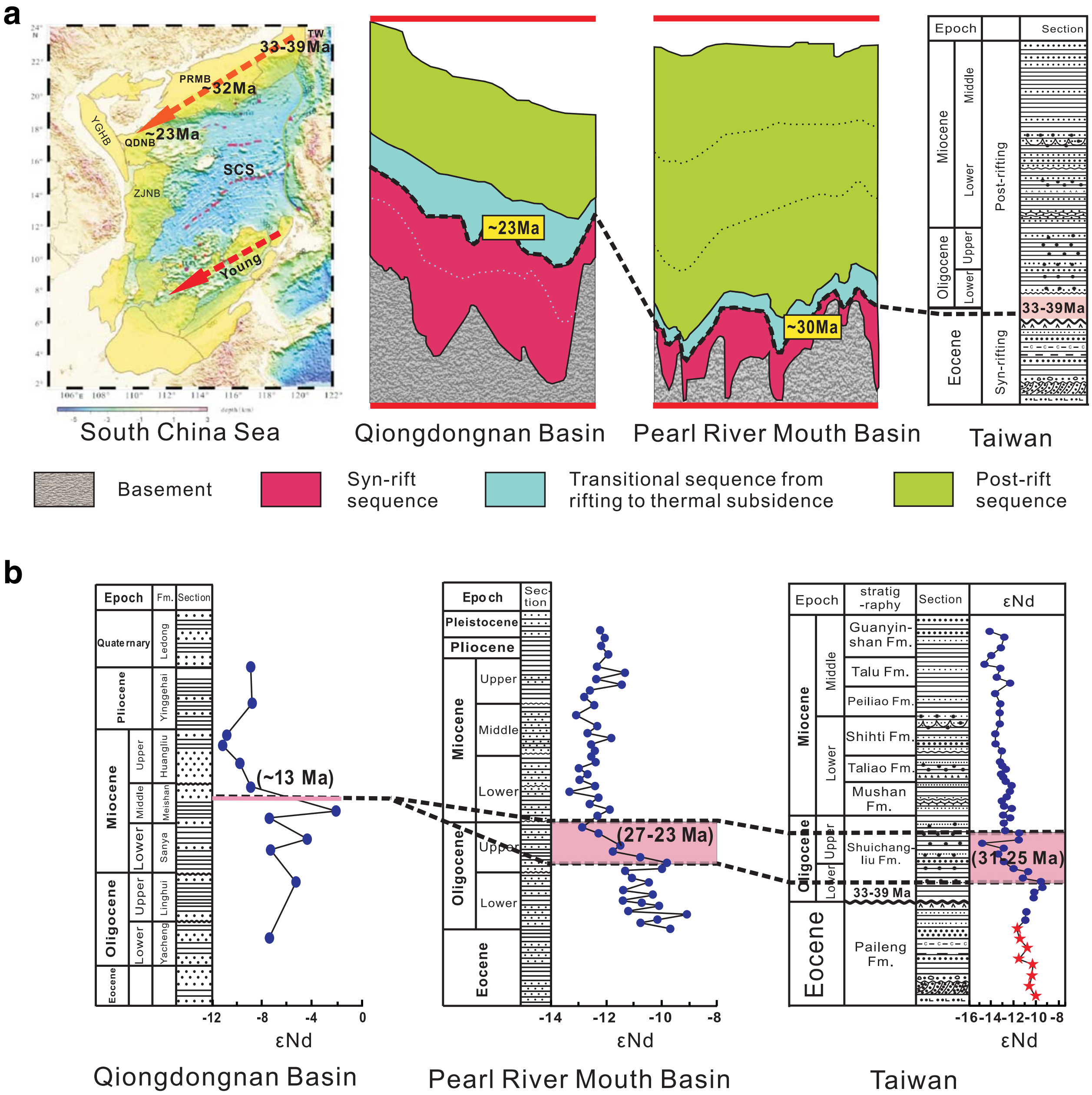

Figure 10. (a) The topography of South China Sea and the varying trend of breakup unconformity and the ages of breakup unconformity in basins around South China Sea. (The Qiongdongnan basin and Pearl River Mouth Basin are represented by the simplified sequence stratigraphic framework of seismic lines). The ages shown near the dotted line refer to the time of breakup unconformity in each basin. TW: Taiwan; PRMB: Pearl River Mouth Basin; QDNB: Qiongdongnan Basin; YGHB: Yinggehai-Song Hong Basin; ZJNB: Zhongjiannan Basin; SCS: South China Sea. (b) εNd variation through time in basins located at the northern periphery of South China Sea, which suggest the change of provenance in these basins. See Figure 2 for the legend of stratigraphic column.

Block once was the most likely source for the exotic sediment to the Red River in the Eocene but the connection was lost prior to 24 Ma. Detrital zircon U-Pb ages from fluvial sediments in the lower reaches of Yangtze River have been used to argue for the development of the modern course of Yangtze between 36.5 and 23 Ma [*Zheng et al*., 2011, 2013]. Although (U-Th)/He thermochronometry from the eastern Tibetan Plateau has demonstrated a major topographic uplift during the Late Miocene [*Clark et al*., 2005; *Godard et al*., 2009], further study based on a variety of thermochronological proxies from this same area revealed that significant exhumation started during Late Oligocene (~30–25 Ma; *Richardson et al*. [2010]; *Wang et al*. [2012]). An outcome of plateau uplift is the readjustment of landscape frameworks and the formation of the large rivers in East Asia [*Wang*, 1998]. Rapid uplift during Oligocene contributed to the eastward-tilting topography required to explain the westward incision of rivers. This also probably aided the small rivers along the eastern coast of Asia to undergo westward capture and gradually become large rivers. Our data from Taiwan show a major shift of provenance starting from ~31 Ma and largely stabilizing after ~25 Ma, which are consistent with these studies in eastern Tibet, although our provenance evolution is not directly connected to uplift of the Tibetan Plateau.

6. Conclusions

In this study, we investigate the initial opening of the South China Sea by investigating the breakup unconformity in Taiwan. SHRIMP U-Pb dating of zircon grains from the Pinglin Tuff indicates that the breakup unconformity formed before 33 Ma, and suggests that seafloor spreading had commenced in South China Sea by that time. Most of the old oceanic crust might have been subducted eastward beneath the Philippine Sea Plate since Late Miocene. The diachronism of breakup unconformities and the transition of provenance in the surrounding rift basins on the northern periphery of South China Sea are consistent with a propagation of seafloor spreading from east to west. The provenance of Cenozoic sequences in Taiwan shows a significant shift. The change of provenance from pre-31 Ma erosion of Phanerozoic arc magmatic rocks exposed along the SE coast of China to post-25 Ma erosion of sources from more inland areas is broadly synchronous with the transition of landscapes and fluvial systems of East Asia, following drainage capture in SW China and SE Tibet driven by progressive uplift of the Tibetan Plateau.

Acknowledgments

We thank M. Santosh for helping to check the English. This work was financially cosupported by the Knowledge Innovation Program of the Chinese Academy of Sciences (grant KZCX2-EW-101), the National Natural Science Foundation of China (grant 41176041, 91128211), and Key Laboratory of Marine Mineral Resources, Ministry of Land and Resources (No.KLMMR-2013-B-04, GZH201200601). This is contribution (GIGRC-10-01) IS-1948 from GIGCAS. Peter D. Clift thanks the Charles T. McCord Jr chair for support to undertake this study.

References

Barckhausen, U., and H. A. Roeser (2004), Seafloor spreading anomalies in South China Sea revisited, in *Continent-Ocean Interactions Within East Asian Marginal Seas*, edited by P. Clift et al., pp. 121–125, AGU, Washington, D. C.

Barckhausen, U., M. Engels, D. Franke, S. Ladage, and M. Pubellier (2014), Evolution of the South China Sea: Revised ages for breakup and seafloor spreading, *Mar. Petrol. Geol.*, in press, doi:10.1016/j.marpetgeo.2014.02.022.

Briais, A., P. Patriat, and P. Tapponnier (1993), Updated interpretation of magnetic anomalies an seafloor spreading stages in the South China Sea: Implications for the tertiary tectonics of Southeast Asia, *J. Geophys. Res.*, *98*, 6299–6328.

Brookfield, M. E. (1998), The evolution of the great river systems of southern Asia during the Cenozoic India–Asia collision; rivers draining southwards, *Geomorphology*, *22*, 285–312.

Chang Y. M. (1963), A biostratigraphic study of small foraminifera from the Wuchi section, Kuohsing, Nantou, Taiwan, *Petrol. Geol. Soc. China*, *2*, 183–207.

Chen, J., and B. M. Jahn (1998), Crustal evolution of southeastern China: Nd and Sr isotopic evidence, *Tectonophysics*, *284*, 101–133.

Chen P. J. (2000), Paleoenvironmental changes during the Cretaceous in eastern China. *Dev. Palaeontol. Stratigr.*, *17*, 81–90.

Chi, W. R. (1979), Calcareous nannoplankton biostratigraphy of the Nantou area, Central Taiwan, *Petrol. Geol. Taiwan*, *16*, 131–165.

Chiu, H. T. (1975), Miocene stratigraphy and its relation to the paleogene rocks in west-central Taiwan, *Petrol. Geol. Taiwan*, *12*, 51–80.

Chou, J. T. (1980), Stratigraphy and sedimentology of the Miocene in western Taiwan, *Petrol. Geol. Taiwan*, *17*, 33–53.

Clark, M. K., L. M. Schoenbohm, L. H. Royden, K. X. Whipple, and B. C. Burchfiel (2004), Surface uplift, tectonics, and erosion of Eastern Tibet from large-scale drainage patterns, *Tectonics*, *23*, TC1006, doi:10.1029/2002TC001402.

Clark, M. K., M. A. House, L. H. Royden, K. X. Whipple, B. C. Burchfiel, X. Zhang, and W. Tang (2005), Late Cenozoic uplift of southeastern Tibet, *Geology*, *33*(6), 525–528.

Clift, P., J. I. Lee, M. K. Clark, and J. Blusztajn (2002), Erosional response of South China to arc rifting and monsoonal strengthening: a record from the South China Sea, *Mar. Geol.*, *184*, 207–226.

Clift, P. D., J. Blusztajn, and D. A. Nguyen (2006), Large-scale drainage capture and surface uplift in Tibet-SW China before 24 Ma inferred from sediments of the Hanoi Basin, Vietnam, *Geophys. Res. Lett.*, *33*, L19403, doi:10.1029/2006GL027772.

Condie, K. C. (1993), Chemical composition and evolution of the upper continental crust: Contrasting results from surface samples and shales, *Chem. Geol.*, *104*, 1–37.

Cullers, R. L. (1994), The controls on the major and trace element variation of shales, siltstones, and sandstones of Pennsylvanian-Permian age from uplifted continental blocks in Colorado to platform sediment in Kansas, USA, *Geochim. Cosmochim. Acta*, *58*(22), 4955–4972.

Cullers, R. L. (2000), The geochemistry of shales, siltstones and sandstones of Pennsylvanian-Permian age, Colorado, USA: Implications for provenance and metamorphic studies, *Lithos*, *51*, 181–203.

Cullers, R. L., and V. N. Podkovyrov (2000), Geochemistry of the Mesoproterozoic Lakhanda shales in southeastern Yakutia, Russia: Implications for mineralogical and provenance control and recycling, *Precambrian Res.*, *104*, 77–93.

Cullers, R. L., S. Chaudhuri, N. Kilbane, and R. Kosh (1979), Rare earths in size fractions and sedimentary rocks of Pennsylvanian: Permian age from the mid-continent of the USA, *Geochim. Cosmochim. Acta*, *43*, 1285–1302.

Darbyshire, D. P. F., and R. J. Sewell (1997), Nd and Sr isotope geochemistry of plutonic rocks from Hong Kong; implications for granite petrogenesis, regional structure and crustal evolution, *Chem. Geol.*, *143*, 81–93.

Falvey, D. A. (1974), The development of continental margins in plate tectonic theory, *APEA J.*, *14*(1), 95–106.

Fedo, C. M., K. N. Sircombe, and R. H. Rainbird (2003), Detrital zircon analysis of the sedimentary record, *Rev. Mineral. Geochem.*, *53*(1), 277–303.

Freydier, R., A. Michard, G. De Lange, and J. Thomson (2001), Nd isotopic compositions of Eastern Mediterranean Sediments: Tracers of the Nile influence during sapropel S1 formation, *Mar. Geol.*, *177*, 45–62.

Gilder, S. A., J. Gill, R. S. Coe, X. Zhao, Z. Liu, G. Wang, K. Yuan, W. Liu, G. Kuang, and H. Wu (1996), Isotopic and paleomagnetic constraints on the Mesozoic tectonic evolution of south China, *J. Geophys. Res.*, *101*(B7), 16,137–16,154.

Gilley, L. D., T. M. Harrison, P. H. Leloup, F. J. Ryerson, O. M. Lovera, and J. H. Wang (2003), Direct dating of left-lateral deformation along the Red River shear zone, China and Vietnam, *J. Geophys. Res.*, *108*(B2), 2127, doi:10.1029/2001JB001726.

Godard, V., R. Pik, J. Lavé, R. Cattin, B. Tibari, J. De Sigoyer, M. Pubellier, and J. Zhu (2009), Late Cenozoic evolution of the central Longmen Shan, eastern Tibet: Insight from (U-Th)/He thermochronometry, *Tectonics*, *28*, TC5009, doi:10.1029/2008TC002407.

Hall, R. (2002), Cenozoic geological and plate tectonic evolution of SE Asia and the SW Pacific: Computer-based reconstructions, model and animations, *J. Asian Earth Sci.*, *20*, 353–431.

Hamilton, P. J., R. K. O'Nions, D. Bridgewater, and A. P. Nutman (1983), Sm-Nd studies of Archean metasedimentts and metavolcanics from west Greenland and their implication for the earth's early history, *Earth Planet. Sci. Lett.*, *62*, 263–272.

Ho, C. S. (1959), Thrust structures in Taichung and Nantou Central Taiwan, *Bull. Geol. Surv. Taiwan*, *11*, 65–80.

Ho, C. S. (1961), Correlation of the Takeng formation and some related stratigraphic principles, *Proc. Geol. Soc. China*, *4*, 61–71.

Ho, C. S., S. F. Tsan, and L. P. Tan (1956), Geology and coal deposit of the Chichitashan area, Nantou, Taiwan, *Geol. Surv. Taiwan Bull.*, *9*, 1–80.

Hoang, L. V., F. Y. Wu, P. D. Clift, A. Wysocka, and A. Swierczewska (2009), Evaluating the evolution of the Red River System based on in-situ U-Pb dating and Hf isotope analysis of zircons, *Geochem. Geophys. Geosyst. 10*, Q11008, doi:10.1029/2009GC002819.

Hsu, S. K., Y. C. Yeh, W. B. Doo, and C. H. Tsai (2004), New bathymetry and magnetic lineations identifications in the northernmost South China Sea and their tectonic implications, *Mar. Geophys. Res.*, *25*(1–2), 29–44.

Hu, D., P. D. Clift, P. Böning, R. Hannigan, S. Hillier, J. Blusztajn, S. Wang, and D. Q. Fuller (2013), Holocene evolution in weathering and erosion patterns in the Pearl River delta, *Geochem. Geophys. Geosyst.*, *14*, 2349–2368, doi:10.1002/ggge.20166.

Huang, C. Y. (1986), Oligocene and Miocene stratigraphy of the Kuohsing Area, central Taiwan, *Acta Geol. Taiwan.*, *24*, 281–318.

Huang, C. Y., and Y. M. Cheng (1983), Oligocene and Miocene planktic foraminiferal biostratigraphy of Northern Taiwan, *Proc. Geol. Soc. China*, *26*, 21–56.

Huang, C. Y., W. Y. Wu, C. P. Chang, S. Tsao, P. B. Yuan, C. W. Lin, and K. Y. Xia (1997), Tectonic evolution of accretionary prism in the arc-continent collision terrane of Taiwan, *Tectonophysics*, *281*, 31–51.

Huang, C. Y., P. B. Yuan, C. W. Lin, T. K. Wang, and C. P. Chang (2000), Geodynamic processes of Taiwan arc-continent collision and comparison with analogs in Timor, Papua New Guinea, Urals and Corsica. *Tectonophysics*, *325*, 1–21.

Huang, C. Y., Y. Yen, P. M. Liew, D. J. He, W. R. Chi, M. S. Wu, and M. Zhao (2012a), Significance of indigenous Eocene Larger Foraminifera *Discocyclina dispansa* in Western Foothills, Central Taiwan: A Paleogene marine rift basin in Chinese continental margin, *J. Asian Earth Sci.*, *62*, 425–437.

Huang, C. Y., Y. Yan, Q. H. Zhao, and C. T. Lin (2012b), Cenozoic stratigraphy of Taiwan: Window into rifting, stratigraphy and paleoceanography of South China Sea, *Chin. Sci. Bull.*, *57*(24), 3130–3149.

Huang, C. Y., W. R. Chi, Y. Yan, K. M. Yang, P. M. Liew, M. S. Wu, J. C. Wu, and C. Zhang (2013), The first record of Eocene tuff in a Paleogene rift basin near Nantou Western Foothills, Central Taiwan, *J. Asian Earth Sci.*, *69*, 3–16.

Huang, T. C., and J. S. Ting (1979), Calcareous nannofossil succession from the Oligocene to Miocene Peikangchi section and revised stratigraphic correlation between northern and central Taiwan, *Proc. Geol. Soc. China*, *22*, 105–120.

Jia, J. T., H. B. Zheng, X. T. Huang, F. Y. Wu, S. Y. Yang, K. Wang, and M. Y. He (2010), Detrital zircon U-Pb ages of Late Cenozoic sediments from the Yangtze delta: Implication for the evolution of the Yangtze River, *Chin. Sci. Bull.*, *55*(15), 1520–1528, doi:10.1007/s11434-010-3091-x.

Kirstein, L. A., A. Carter, and Y. G. Chen (2010), Testing inferences from palaeocurrents: Application of zircon double-dating to Miocene sediments from the Hengchun Peninsula, Taiwan, *Terra Nova*, *22*(6), 483–493.

Lan, C. Y., S. L. Chung, T. Van Long, C. H. Lo, T. Y. Lee, S. A. Mertzman, and J. Jiun-San Shen (2003), Geochemical and Sr–Nd isotopic constraints from the Kontum massif, central Vietnam on the crustal evolution of the Indochina block, *Precambrian Res.*, *122*(1), 7–27.

Leloup, P. H., N. Arnaud, R. Lacassin, J. R. Kienast, T. M. Harrison, T. T. Trong, and P. Tapponnier (2001), New constraints on the structure, thermochronology, and timing of the Ailao Shan-Red River shear zone, SE Asia, *J. Geophys. Res.*, *106*(B4), 6683–6732.

Li, J., S. Xie, and M. Kuang (2001), Geomorphic evolution of the Yangtze Gorges and the time of their formation, *Geomorphology*, *41*, 125–135.

Li, X., C. Qi, Y. Liu, X. Liang, X. Tu, L. Xie, and Y. Yang (2005), Petrogenesis of the Neoproterozoic bimodal volcanic rocks along the western margin of the Yangtze Block: New constraints from Hf isotopes and Fe/Mn ratios, *Chin. Sci. Bull.*, *50*(21), 2481–2486.

Li, X. H., M. Sun, G. J. Wei, Y. Liu, C. Y. Lee, and J. Malpas, (2000), Geochemical and Sm–Nd isotopic study of amphibolites in the Cathaysia Block, southeastern China: Evidence for an extremely depleted mantle in the Paleoproterozoic, *Precambrian Res.*, *102*(3), 251–262.

Li, X. H., G. J. Wei, L. Shao, Y. Liu, X. Liang, Z. Jian, M. Sun, and P. X. Wang (2003), Geochemical and Nd Isotopic variations in sediments of the South China Sea: A response to Cenozoic tectonism in SE Asia, *Earth Planet. Sci. Lett.*, *211*, 207–220.

Li, X. H., D. Y. Liu, M. Sun, W. X. Li, X. R. Liang, and Y. Liu, (2004), Precise Sm–Nd and U–Pb isotopic dating of the super-giant Shizhuyuan polymetallic deposit and its host granite, *Southeast China Geol. Mag.*, *141*, 225–231.

Li, X. H., Y. Liu, Q. L. Li, C. H. Guo, and K. R. Chamberlain (2009), Precise determination of Phanerozoic zircon Pb/Pb age by multicollector SIMS without external standardization, *Geochem. Geophys. Geosyst.*, *10*, Q04010, doi:10.1029/2009GC002400.

Liu, J., Z. Sun, Y. Liu, Z. Zhao, and Z. Wang (2012), Progress of Cenozoic tectonic studies in Qiongdongnan Basin [in Chinese with English abstract], *Mar. Geol. Frontiers*, *28*(4), 1–9.

Lüdmann, T., and H. K. Wong, (1999), Neotectonic regime on the passive continental margin of the northern South China Sea, *Tectonophysics*, *311*(1), 113–138.

Ma, C., C. Ehlers, C. Xu, Z. Li, and K. Yang (2000), The roots of the Dabieshan ultrahigh-pressure metamorphic terrane: Constraints from geochemistry and Nd-Sr isotope systematics, *Precambrian Res.*, *102*, 279–301.

McCulloch, M. T., and G. J. Wasserburg (1978), Sm-Nd and Rb-Sr chronology of continental crust formation, *Science*, *200*(4345), 1003–1011, doi:10.1126/science.200.4345.1003.

Nagel, S., S. Castelltort, A. Wetzel, S. D. Willett, F. Mouthereau, and A. T. Lin (2013), Sedimentology and foreland basin paleogeography during Taiwan arc continent collision, *J. Asian Earth Sci.*, *62*, 180–204.

Peltzer, G., and P. Tapponnier (1988), Formation and evolution of strike-slip faults, rifts, and basins during the India-Asia collision: An experimental approach, *J. Geophys. Res. 93*(B12), 15,085–15,117.

Richardson, N. J., A. L. Densmore, D. Seward, A. Fowler, M. Wipf, M. A. Ellis, Y. Li, and Y. Zhang (2008), Extraordinary denudation in the Sichuan Basin: Insights from low-temperature thermochronology adjacent to the eastern margin of the Tibetan Plateau, *J. Geophys. Res.*, *113*, B04409, doi:10.1029/2006JB004739.

Richardson, N. J., A. L. Densmore, D. Seward, M. Wipf, and Y. Li (2010), Did incision of the Three Gorges begin in the Eocene?, *Geology*, *38*(6), 551–554.

Rowley, D. B. (1996), Age of initiation of collision between India and Asia: A review of stratigraphic data, *Earth Planet. Sci. Lett.*, *145*, 1–13.

Shao, L., X. Pang, C. M. Chen, H. S. Shi, Q. Y. Li, and P. J. Qiao (2007), Terminal Oligocene sedimentary environments and abrupt provenance change event in the northern South China Sea [in Chinese with English abstract], *Geol. China*, *34*(6), 1022–1031.

Shao, L., P. J. Qiao, X. Pang, G. J. Wei, Q. Y. Li, W. L. Miao, and A. Li (2009), Nd isotopic variations and its implications in the recent sediments from the northern South China Sea [in Chinese with English abstract], *Chin. Sci. Bull.*, *54*(2), 311–317, doi:10.1007/s11434-008-0453-8.

Sharp, W. D., and D. A. Clague (2006), 50-Ma initiation of Hawaiianemperor bend records major change in Pacific plate motion, *Science*, *313*, 1281–1284.

Suppe, J. (1984), Kinematics of arc-continent collision, flipping of subduction, and back-arc spreading near Taiwan, *Mem. Geol. Soc. China*, *6*, 21–34.

Tan, L. P., and C. C. Youh (1978), Characteristics and paleogeographic environment of the metamorphosed high-purity sandstone deposits in Taiwan, *Proc. Geol. Soc. China*, *21*, 92–100.

Tapponnier, P., G. Peltzer, and R. Armijo (1986), On the mechanics of the collision between India and Asia, in *Collision Tectonics*, *Geol. Soc. Spec. Publ.*, edited by M. P. Coward and A. C. Ries, *19*(1), pp. 115–157, Geological Society, London, U. K.

Taylor, B., and D. E. Hayes (1980), The tectonic evolution of the south China Basin, *Geophys. Monogr. Ser.*, *23*, 89–104.

Taylor, B., and D. E. Hayes (1983), Origin and history of the South China Sea basin, in *The Tectonic and Geologic Evolution of Southeast Asian Seas and Islands: Part 2, Geophys. Monogr. Ser. 27*, edited by D. E. Hayes, pp. 23–56, AGU, Washington, D. C.

Taylor, S. R., and S. M. McLennan (1985), *The continental Crust: Its Composition and Evolution*, pp. 2–57, Blackwell Sci., Oxford.

Tera, F., and G. J. Wasserburg (1972), U–Th–Pb systematics in three Apollo 14 basalts and the problem of initial Pb in lunar rocks, *Earth Planet. Sci. Lett.*, *14*, 281–304.

Wang C., X. Li, X. Hu, and L. F. Jansa (2002), Latest marine horizon north of Qomolangma (Mt Everest): Implications for closure of Tethys seaway and collision tectonics, *Terra Nova*, *14*(2), 114–120.

Wang, E., E. Kirby, K. P. Furlong, M. van Soest, G. Xu, X. Shi, P. J. J. Kamp, and K. V. Hodges (2012), Two-phase growth of high topography in eastern Tibet during the Cenozoic, *Nat. Geosci.*, *5*(9), 640–645.

Wang, P. X. (1998), Deformation of Asia and global cooling: Searching links between climate and tectonics [in Chinese with English abstract], *Quat. Sci.*, *3*, 213–221.

Wang, P. X. (2005), Cenozoic deformation and history of sea-land interactions in Asia [in Chinese with English abstract], *J. China Univ. Geosci.*, *30*(1), 1–18.

Wang, P. X., Q. Zhao, Z. Jian, X. Cheng, W. Huang, J. Tian, J. Wang, Q. Li, B. Li, and X. Su (2003), Thirty million year deep sea records in the South China Sea, *Chin. Sci. Bull.*, *48*(23), 2524–2535.

Wei, G. J., Y. Liu, X. H. Li, L. Shao, and D. Y. Fang (2004), Major and trace element variations of the sediments at ODP1144, South China Sea, during the last 230Ka and their paleoclimate implications, *Palaeogeogr. Palaeoclimatol. Palaeoecol.*, *212*, 331–342.

Wiedenbeck, M., P. Alle, F. Corfu, W. L. Griffin, M. Meier, F. Oberli, A. Vonquadt, J. C. Roddick, and W. Speigel (1995), Three natural zircon standards for U-Th-Pb, Lu-Hf, trace-element and REE analyses, *Geostand. Newsl.*, *19*, 1–23, doi:10.1111/j.1751-908X.1995.tb00147.x.

Wu, F. Y., W. Q. Ji, C. Z. Liu, and S. L. Chung (2010), Detrital zircon U–Pb and Hf isotopic data from the Xigaze fore-arc basin: Constraints on Transhimalayan magmatic evolution in southern Tibet. *Chem. Geol.*, *271*(1), 13–25.

Yan, Y., B. Xia, G. Lin, A. Carter, X. Q. Hu, X. Cui, B. Liu, P. Yan, and Z. Song (2007), Geochemical and Nd Isotope composition of detrital sediments on the north margin of the South China Sea: Provenance and tectonic implications, *Sedimentology*, *54*, 1–17, doi:10.1111/j.1365-3091.2006.00816.x.

Yan, Y., A. Carter, C. Palk, S. Brichau, and X. Hu (2011), Understanding sedimentation in the Song Hong–Yinggehai Basin, South China Sea, *Geochem. Geophys. Geosyst.*, *12*, Q06014, doi:10.1029/2011GC003533.

Yan, Y., A. Carter, C. Y. Huang, L. S. Chan, X. Q. Hu, and Q. Lan (2012), Constraints on Cenozoic regional drainage evolution of SW China from the provenance of the Jianchuan Basin, *Geochem. Geophys. Geosyst.*, *13*, Q03001, doi:10.1029/2011GC003803.

Yang S., C. Li, and K. Yokoyama (2006), Elemental compositions and monazite age patterns of core sediments in the Changjiang Delta: Implications for sediment provenance and development history of the Changjiang River, *Earth Planet. Sci. Lett.*, *245*, 762–776.

Yang, S., S. Jiang, H. Ling, X. Xia, M. Sun, and D. Wang (2007), Sr-Nd isotopic compositions of the Changjiang sediments: Implications for tracing sediment sources, *Sci. China Ser. D Earth Sci.*, *50*(10), 1556–1565.

Yang, T. F., J. L. Tien, C. H. Chen, T. Lee, and R. S. Punongbayan (1995), Fission-track dating of volcanics in the northern part of the Taiwan-Luzon Arc: Eruption ages and evidence for crustal contamination, *J. Southeast Asian Earth Sci.*, *11*(2), 81–93.

Yao, B. C. (1997), The sea floor spreading in the SW subbasin of South China Sea and it's tectonic significance [in Chinese with English abstract], *Geol. Res. South China Sea*, *9*, 20–36.

Yao, B. C., W. J. Zeng, Y. Z. Chen, X. L. Zhang, D. E. Hayes, J. Diebold, P. Bubl, and S. Spangler (1994), The Crustal structure in the eastern Part of the northern margin of the South China Sea [in Chinese with English abstract], *Acta Geophys. Sin.*, *37*(1), 27–35.

Yokoyama, K., Y. Tsutsumi, C. S. Lee, J. J. S. Shen, C. Y. Lan, and L. Zhao (2007), Provenance study of Tertiary Sandstones from the Western Foothills and Hsuehshan Range, Taiwan, *Bull. Natl. Mus. Nat., Sci. Ser. C*, *33*, 7–26.

Yu, S. B., H. Y. Chen, and L. C. Kuo (1997), Velocity field of GPS stations in the Taiwan area, *Tectonophysics*, *274*(1), 41–59.

Zheng, H., D. Jia, J. Chen, and P. Wang (2011), Did incision of the Three Gorges begin in the Eocene?, *Geology*, *39*(9), e244, doi:10.1130/G31944C.1.

Zheng, H. B., P. D. Clift, P. Wang, R. Tada, J. Jia, M. He, and F. Jourdan (2013), Pre-Miocene birth of the Yangtze River, *Proc. Natl. Acad. Sci. U. S. A.*, *110*(19), 7556–7561.

Zhou, D., K. Ru, and H. Z. Chen (1995), Kinematics of Cenozoic extension on the South China Sea continental margin and its implications for the tectonic evolution of the region, *Tectonophysics*, *251*, 161–177.

